Supporting information Novel Feathery P/S co-doped Graphitic Carbon Nitride for Highly Efficient Synergistic Photocatalytic H_2O_2-generation and Tetracycline-degradation

S1 Experimental Section

Preparation of g-C_3N_4 by the hydrothermal method (CN) :

The molar ratio of 1:1 melamine (MA) and cyanuric acid (CA) were dissolved in 50 mL of deionized water, respectively. The solution was stirred in a water bath at 80 °C until it became colorless. Subsequently, the melamine and melinic acid solutions were mixed together and stirred for 40 min. After cooling, the mixture was centrifuged at high speed to obtain melamine solution and melinic acid complexes (MA-CA). The MA-CA complexes was then redispersed into 70 mL of deionized water and stirred for 30 min. The resulting mixed solution was transferred to a 100 mL PTFE stainless steel autoclave for reaction at 150 °C for 10 h. Following this, the white compound was centrifuged and washed several times with ethanol and deionized water, dried under vacuum at 60 °C for 24 h to obtain the MCA precursor after grinding. Finally, the MCA precursor was placed in a porcelain boat with lid in a tube furnace with nitrogen atmosphere and calcined at 520 °C for 2 h before naturally cooled to room temperature to yield the CN photocatalyst.

Preparation of g-C_3N_4 by the calcination method :

Melamine was placed in a covered porcelain boat in a tubular furnace, the atmosphere was nitrogen, calcined at 520°C for 2 h, and naturally cooled to room temperature to obtain a bulk g-C3N4 photocatalyst.

Synthesis of P-doped CN (P_x-CN):

MA-CA was redispersed into 70 mL of deionized water, and various amounts of ammonium dihydrogen phosphate (PA) were added while stirring for 30 min. The mixed solution was then transferred to an autoclave and reacted at 150 °C for 10 h. Subsequently, the P_x-MCA precursors were obtained through centrifugation, washing, drying, and grinding process. The masses of ammonium dihydrogen phosphate used were 0.1 g, 0.3 g, 0.5 g, and 0.8 g, respectively, corresponding to the labels $P_{0.1}$-MCA, $P_{0.3}$-MCA, $P_{0.5}$-MCA, and $P_{0.8}$-MCA, respectively. The P_x-MCA precursors were placed in a covered porcelain boat in a tube furnace with a nitrogen atmosphere and calcined at 520 °C for 2 h before being naturally cooled to room temperature to obtain Different P_x-CN photocatalysts were obtained.

Synthesis of S-doped CN (S_y-CN):

MA-CA was redispersed into 70 mL of deionized water, and different masses of thiourea (TU) was added during stirring for 30 min. The mixed solution was transferred to an autoclave for reaction at 150 °C for 10 h. Subsequently, The S_y-MCA precursors were obtained by centrifugation, washing, drying, and grinding. Thiourea masses of 0.1 g, 0.2 g, 0.4 g, and 0.6 g were used and labeled as $S_{0.1}$-MCA, $S_{0.2}$-MCA, $S_{0.4}$-MCA, and $S_{0.6}$-MCA. The Sx-MCA precursors were placed in a covered porcelain boat in a tube furnace with nitrogen atmosphere and calcined at 520 °C for 2 h. Finally, the precursors were naturally cooled to room temperature to obtain different S_y-CN photocatalysts.

Synthesis of P and S co-doped CN (P_xS_y-CN):

MA-CA was redispersed into 70 mL of deionized water, and varying amounts of ammonium dihydrogen phosphate and thiourea were added while stirring for 30 min. The mixed solution was transferred to an autoclave for reaction at 150 °C for 10 h. Subsequently, P_xS_y-MCA precursor was obtained by centrifugation, washing, drying, and grinding. Ammonium dihydrogen phosphate weighing 0.3 g and thiourea mass of 0.2 g were labeled as $P_{0.3}S_{0.2}$-CN. The different P_xS_y-CN precursors

were obtained by placing the P_xS_y-CMA precursors in a covered porcelain boat in a tube furnace with nitrogen atmosphere and calcined at 520 °C for 2 h and naturally cooled to room temperature.

S2 Evaluation of H_2O_2 photocatalytic production

The photocatalyst was dissolved in 50 mL of aqueous solution (containing 10% isopropanol), followed by sonication for 3 min and stirring for 30 min under light-proof conditions. Continuous feeding of O_2 was carried out to reach the adsorption-desorption equilibrium. The distance between the light source and the reactor was kept at a fixed value throughout the experiment, while the temperature was kept at 25 °C. Prior to the photocatalytic reaction, the Xe lamp was generally preheated for 30 min, and a small amount of O_2 was introduced into the solution during the entire reaction process. Taking the mixed solution at 30 min intervals, filtered through a 0.22 μm membrane, and the supernatant was centrifuged (8000 rpm·min-1, 10 min) to measure the concentration of H_2O_2 by iodometric measurement. The standard curve of H_2O_2 was obtained by UV-Vis spectrophotometer at a wavelength of 350 nm after equilibrated. The concentrations of H_2O_2 produced by different carbon nitrides were obtained from the standard curve.

The H_2O_2 was decomposed as follows: the Xe lamp was preheated, the photocatalyst was put into H_2O_2 of known concentration (a) without adding hydrogen source (isopropanol), and the supernatant was obtained by filtration and centrifugation of the mixed solution at 30 min intervals. A blank group was set up and H_2O_2 was substituted for H_2O, and the above steps were repeated to measure the concentration (c). The final decomposition efficiency $\eta(H_2O_2)$ is shown in Equation 1.1.

$$\eta(H2O2) = \frac{a - b + c}{a} \times 100\% \tag{S1.1}$$

Stability test of photocatalytic H_2O_2 production: H_2O_2 in a 50 mL solution (containing 10% isopropanol) using 50 mg of photocatalyst was performed for repeatedly replicate experiments.

S3 Evaluation of Photocatalytic oxidation-Fenton oxidation for TC degradation

The photocatalyst was dispersed into 50 mL of TC solution (10 ~ 80 mg·L-1) and stirred in the dark for 30 min to reach adsorption-desorption equilibrium with the antibiotic TC. The LED lamp disc (λ = 420 nm) generally needs to be preheated for 5 min before the photocatalytic reaction. The whole experiment was controlled at 25 °C, and a small amount of oxygen was introduced into the reaction flask. After illuminating for 60 min, 1.6 mg $FeSO_4 \cdot 7H_2O$ was added to the solution, and the reaction was stopped until 100 min. The stirring speed was set at 100 rpm·min-1. During the degradation of TC, the mixed solution was taken every 20 min, filtered through a 0.22 μm membrane, and the supernatant was taken by centrifugation (8000 rpm·min-1, 10 min). The absorbance of TC was measured using UV-Vis spectrophotometer and the degradation efficiency was calculated. The photodegradation efficiency (η_{eff}) of TC solution was determined according to Equation 1.2:

$$\eta eff = (1 - \frac{C_t}{C_0}) \times 100\% = (1 - \frac{A_t}{A_0}) \times 100\% \tag{S1.2}$$

The above experiments were repeated for the carbon nitride selected for the best photocatalytic performance, and the solutions were taken for each fixed time period and detected by High Performance Liquid Chromatography-Quadrupole-Time of Flight-Mass Spectrometry (HPLC-Q-TOF-MS). HPLC-Q-TOF-MS) and quenched with methanol prior to detection. Photocatalytic degradation intermediates can be detected by HPLC-Q-TOF/ESI-MS/MS in selective reaction monitoring

mode.

Kinetic analysis of photocatalytic degradation

Assessing the photocatalytic performance of carbon nitride can be made more intuitive by analyzing the kinetics. In general, the Langmuir-Hinshelwood kinetic model is used to represent the reaction of organic pollutants on the photocatalyst. The rate of photocatalytic antibiotic degradation is shown in Equation S1.3:

$$r = k_r = -\frac{dc}{dt} = k_r \frac{K_a C}{1 + K_a} \times 100\% \qquad (S1.3)$$

where r is the photocatalytic degradation rate, kr reflects the true rate constant, and Ka is the adsorption constant. At low initial concentrations (KaC << 1), the KaC in Eq. is generally negligible, in accordance with the following pseudo primary kinetic model (Eqs. S1.4 and S1.5):

$$r = -\frac{dc}{dt} = k_r k_a t \times 100\% = k_{pfo} t \qquad (S1.4)$$

This kinetic model can be simplified as follows:

$$\ln = k_r k_a t \times 100\% = k_{pfo} t \qquad (S1.5)$$

C_0 and C_t and are the initial concentration and concentration of TC ($mg \cdot L^{-1}$), kpfo is the quasi-primary reaction rate constant for photodegradation of TC (min^{-1}), and t is the reaction time for photodegradation (min)[1, 2].

S4 Characterization

In the experimental process, the microscopic morphology of the synthesized materials was primarily observed and recorded using a field emission scanning electron microscope (SEM, ULTRA plus), a transmission electron microscope (TEM, TECNAI-G2-TF20), and a high-resolution transmission electron microscope (HRTEM). The crystal lattice details were captured with the high-resolution transmission electron microscope (High-resolution TEM). Additionally, the atomic structure and elemental composition of the materials were precisely analyzed using an energy dispersive X-ray spectroscope (EDS, Oxford X-max 20). The qualitative analysis of the crystal structure of the synthesized materials was mainly performed using X-ray powder diffraction (XRD, Bruker AXS D8 Advance, Cu-Kα, λ = 1.5406 Å, 2θ range of 10° to 70°, scan rate: 2 °C·min^{-1}).

The elemental composition, atomic valence states, chemical bonds, and contents of the synthesized materials were analyzed using X-ray photoelectron spectroscopy (XPS, ESCAlab250iX, with a monochromator resolution of ≤ 0.45 eV). The surface functional groups and chemical bonds of the synthesized materials were qualitatively analyzed using Fourier-transform infrared spectroscopy (FT-IR, 200VCE, with a wavenumber range of 500 to 4000 cm−1, resolution of 4 cm^{-1}, and a single scan exposure time of 30 s). The specific surface area of all synthesized samples was measured using the Brunauer-Emmett-Teller (BET) equation at a temperature of 373 K (N_2 environment, Quadrasorb SI, Quantachrome, USA).

The optical properties of the materials were analyzed and measured using a solid UV-Vis diffuse reflectance spectroscopy (UV-vis-DRS) spectrophotometer (Shimadzu UV-3600, Japan). Residual organic molecules from antibiotic steps were quantitatively analyzed using a UV spectrophotometer (UV-3900, Shimadzu, Japan). Additionally, optical

properties (excitation wavelength λ = 360 nm) were tested and analyzed using photoluminescence (PL, RF-6000, Shimadzu, Japan) spectroscopy and time-resolved photoluminescence (TRPL, FLS980, Edinburgh Instruments, UK). The electronic spin resonance signals of radicals were measured using an electron spin resonance spectrometer (EPR, Bruker E500, visible light wavelength λ > 420 nm, spin trapping reagent: 5-dimethyl-L-pyrroline-N-oxide (DMPO)).

S5 Photocurrent and EIS measurements

Photocurrent and EIS measurements were conducted using an electrochemical workstation (CHI-760, China). A standard three-electrode setup was used, with a Pt electrode as the working electrode and a saturated calomel electrode (SCE) as the reference electrode. The working electrode preparation steps are as follows: 5 mg of the sample was dispersed in 950 μL of anhydrous ethanol and 100 μL of Nafion solution to form a slurry, which was then dropped onto a 0.25 cm² FTO substrate and vacuum-dried at 60°C for 24 hours. The electrolyte for photocurrent measurements was a 0.1 M Na_2SO_4 solution, and the light source was a 300 W Xe lamp (λ > 420 nm). Electrochemical impedance spectroscopy (EIS) was performed over a frequency range of 1.0×10^5 to 0.01 Hz, with a sine wave perturbation amplitude of 5.0 mV at a potential bias of 0.2 eV vs. SCE. The electrolyte for impedance testing was a mixed solution of 1 mM $K_3Fe(CN)_6$, 1 mM $K_4Fe(CN)_6 \cdot 3H_2O$, and 0.1 M KCl.

S6 DFT calculation methods

In this study, generalized gradient approximation (GGA) was used to calculate all spin polarization density functional theory (DFT) using the first-principles Perdew-Burke-Ernzerhof (PBE) formulation. The plane wave pseudopotential (PAW) was chosen to describe the interaction between the nucleus and the electron, and the truncated energy of the plane wave group is 450 eV. In the geometric optimization, the convergence criteria for the energy and force of the self-consistent field are set to 1×10^{-5} eV and 0.02 eV/A, respectively, and the K point of the gamma grid selected in the reciprocal space Brillouin region is 2×2×1.
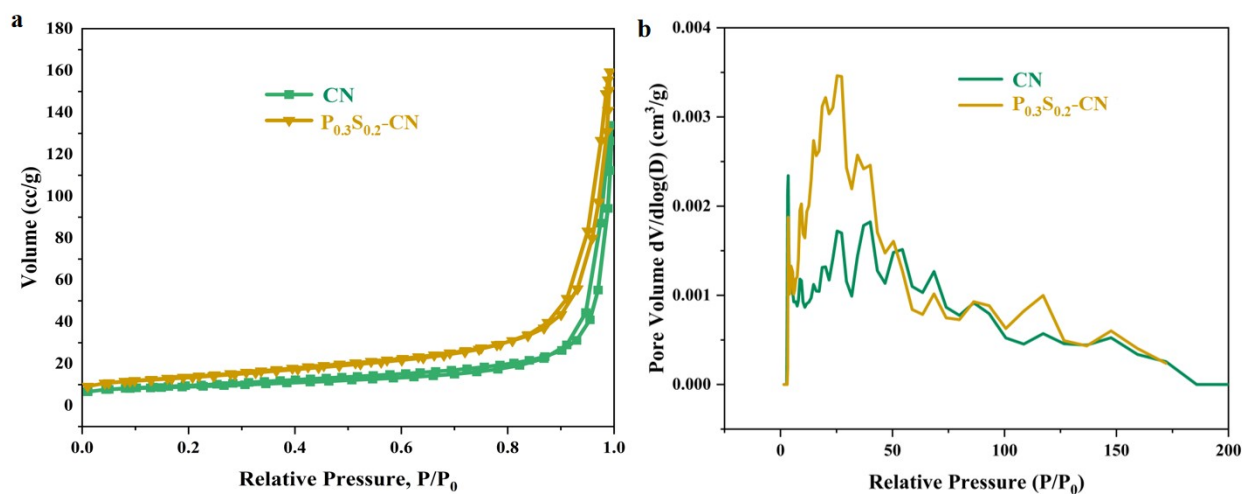
Figure S1. CN and PS-CN of (a) N_2 adsorption and desorption isotherms and, (d) BJH pore size distribution. In the range of relative pressure 0 to 1.0, both CN and $P_{0.3}S_{0.2}$-CN catalysts exhibit type IV adsorption isotherms according to the IUPAC

classification, with the hysteresis loop occurring around 1.0. This indicates the presence of mesoporous structures in the samples. A significant change in adsorption capacity when P/P$_0$ increases to 0.85 to 1.0 suggests the presence of capillary condensation. As shown in Figure S1a, the pore size distribution of the samples was obtained using Barrett-Joyner-Halenda (BJH) analysis. The specific surface areas of CN and P$_{0.3}$S$_{0.2}$-CN are 33.45 and 48.23 m²·g⁻¹, respectively, with corresponding pore sizes of 24.74 and 20.43 nm. The specific surface area of P$_{0.3}$S$_{0.2}$-CN is 5.84 times greater than that of the g-C$_3$N$_4$ prepared in the literature (8.25 m²·g⁻¹) [3].
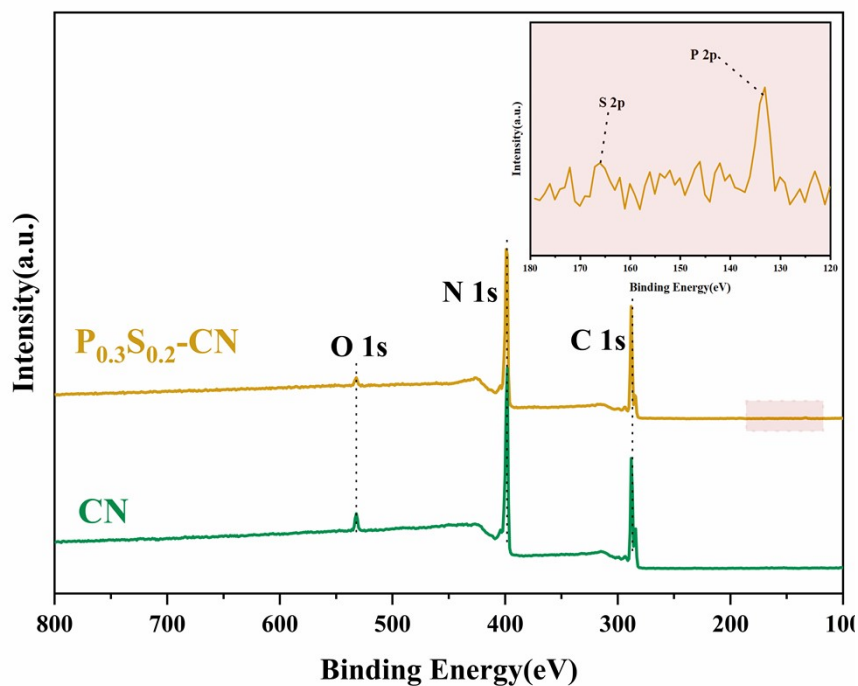
Figure S2. XPS scanning spectra of CN and P$_{0.3}$S$_{0.2}$-CN.
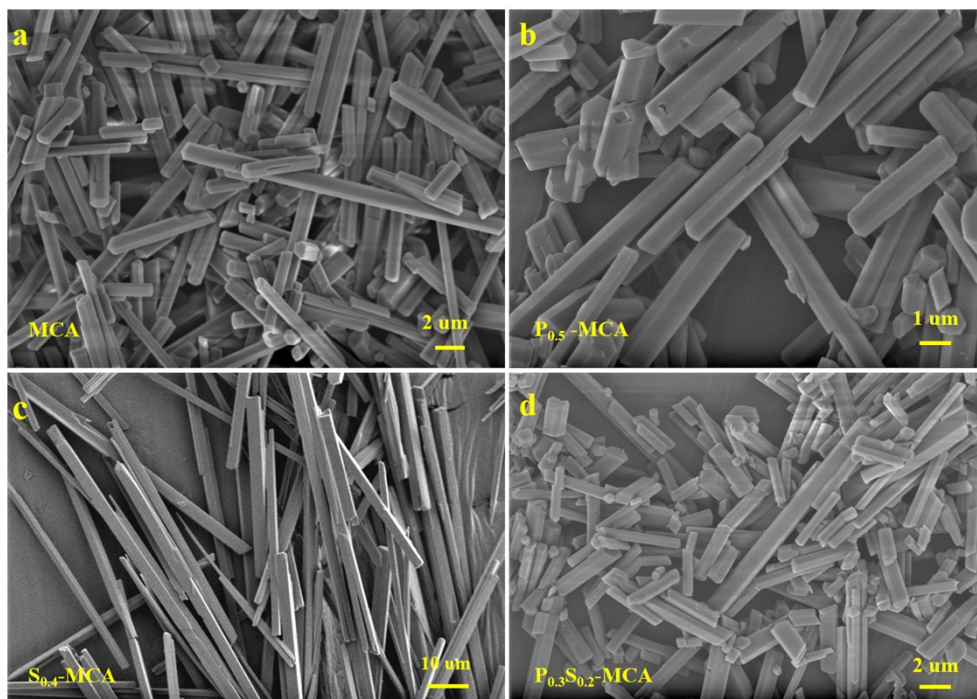
Figure S3. SEM images of (a) MCA, (b) $P_{0.5}$-MCA, (c) $S_{0.4}$-MCA and (d)$P_{0.3}S_{0.2}$-MCA.
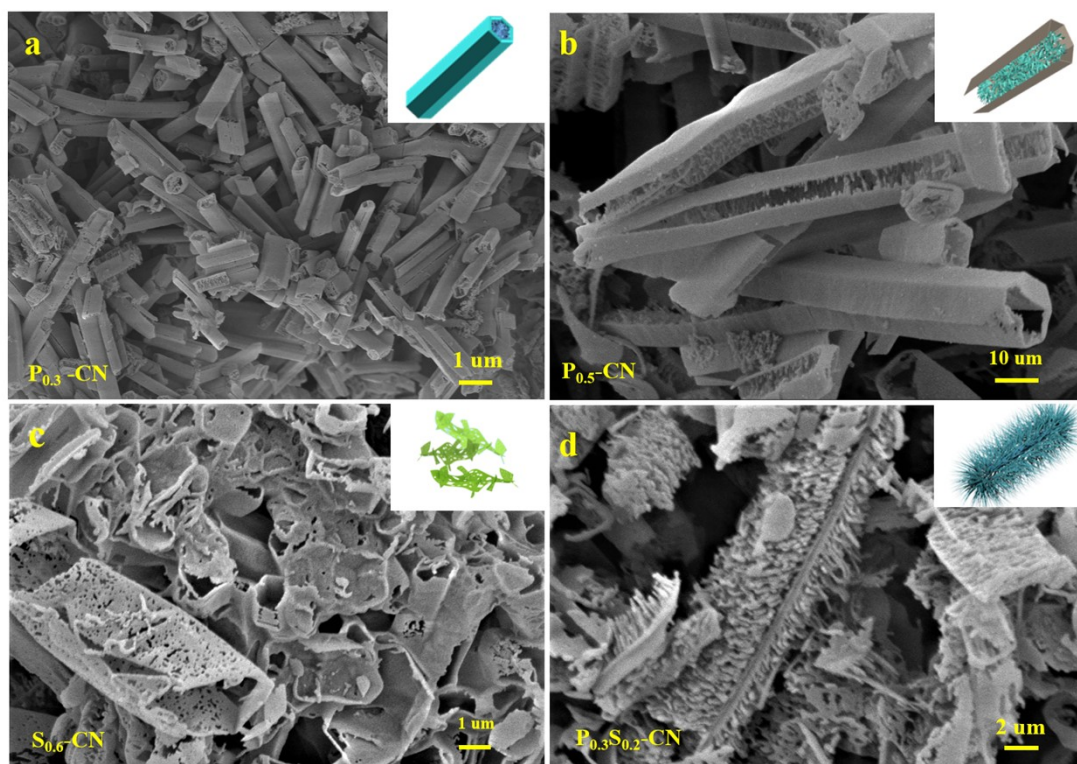
Figure S4. SEM images of (a)$P_{0.5}$-CN, (b)$P_{0.3}$-CN, (c)$S_{0.6}$-CN with (d)$P_{0.3}S_{0.2}$-CN.
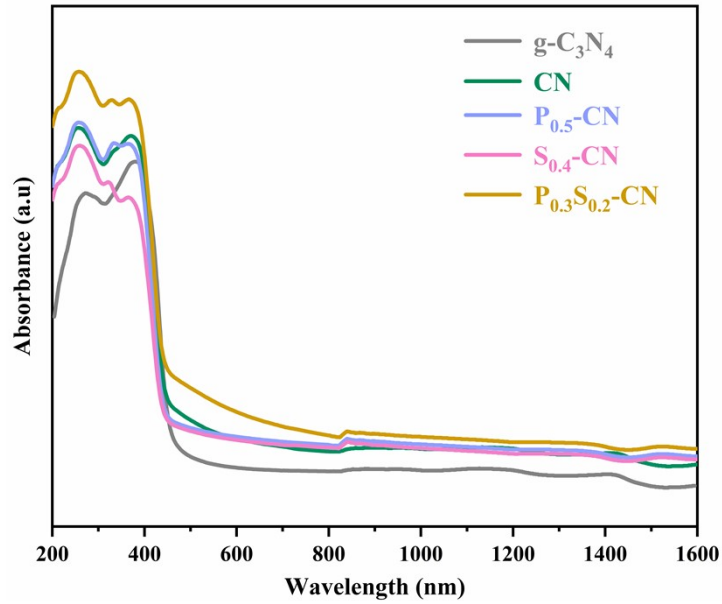
Figure S5. UV-Vis DRS plots of $g-C_3N_4$, CN, $P_{0.5}-CN$, $S_{0.4}-CN$, and $P_{0.3}S_{0.2}-CN$.
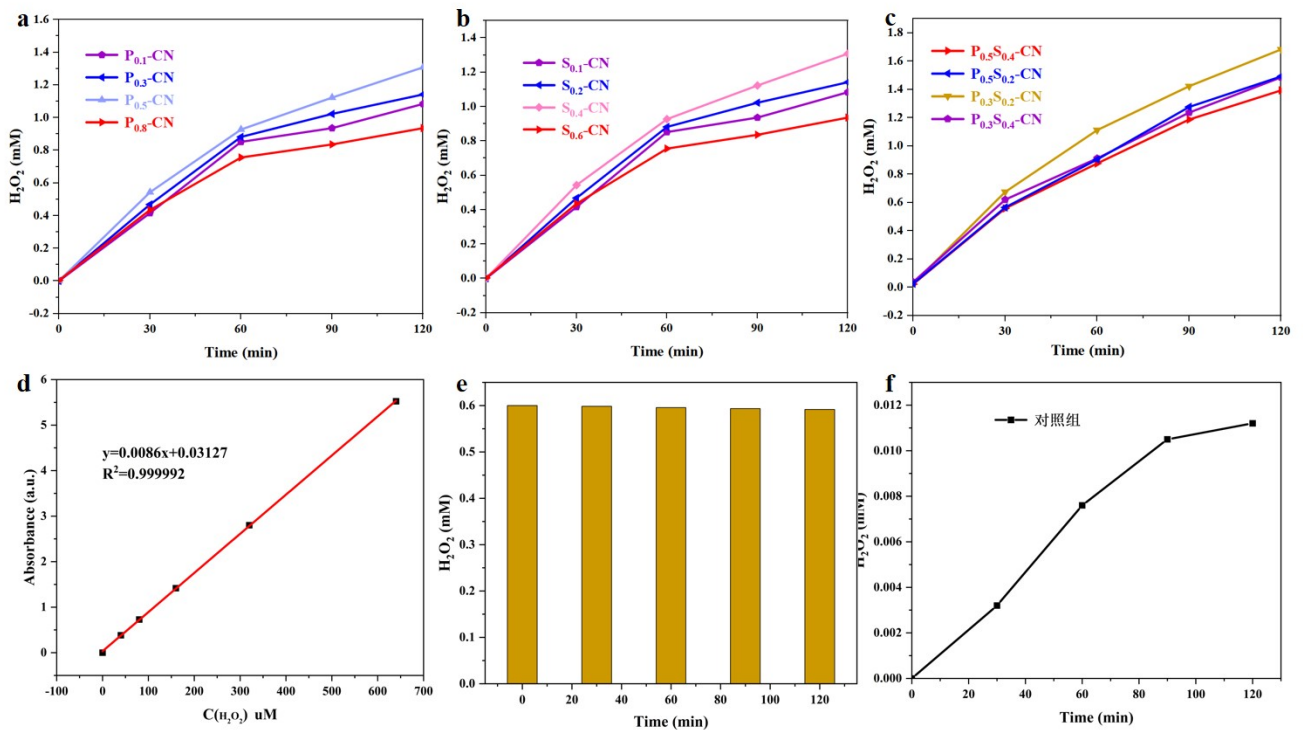
Figure S6. Photocatalytic H_2O_2 yields of (a) different amounts of P-doped CN, (b) different amounts of S-doped CN, (c) different amounts of P and S-doped CN , (d) Standard curve of H_2O_2, (e) Photocatalytic decomposition of H_2O_2, (f) blank control experiment.
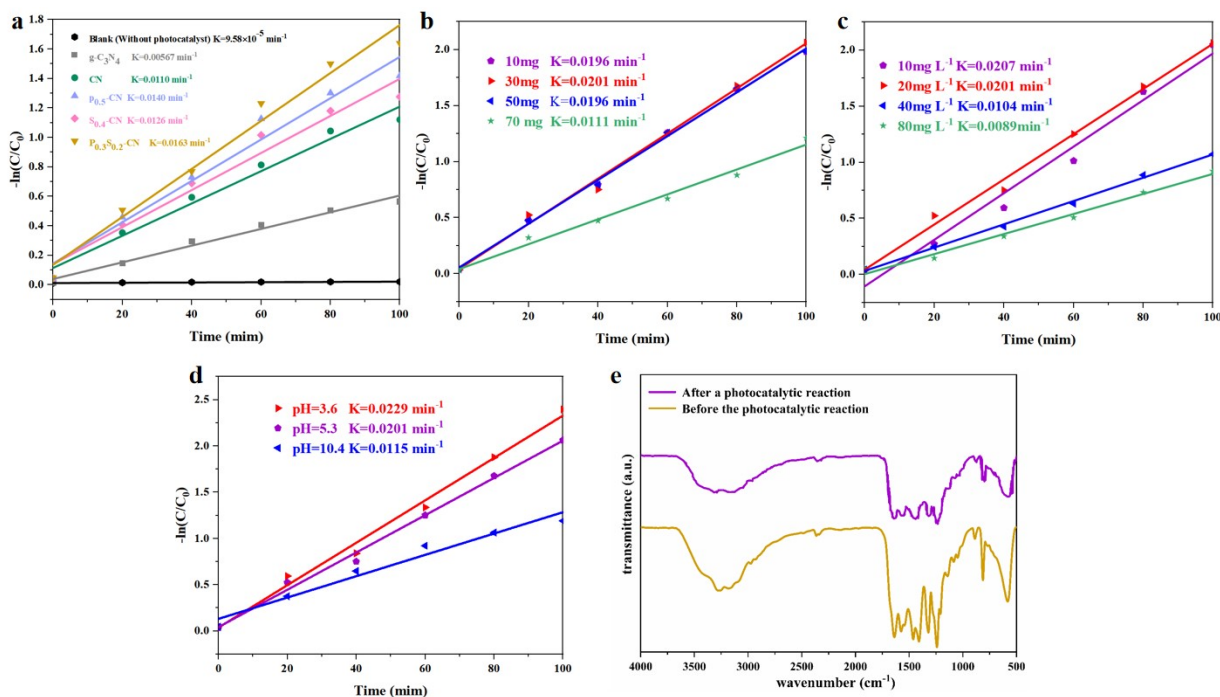
Figure S7. Under visible light irradiation (a) Photocatalytic oxidative degradation of TC (20 mg/L) by different catalysts (30 mg), (b) Effect of the amount of PS-CN, (c) initial concentration of TC, (d) different pH on photocatalytic oxidation-Fenton oxidative degradation corresponding kinetic curves, (e) the Fourier-transform infrared spectrum of $P_{0.3}S_{0.2}$ after four cycles of photocatalytic experiments.
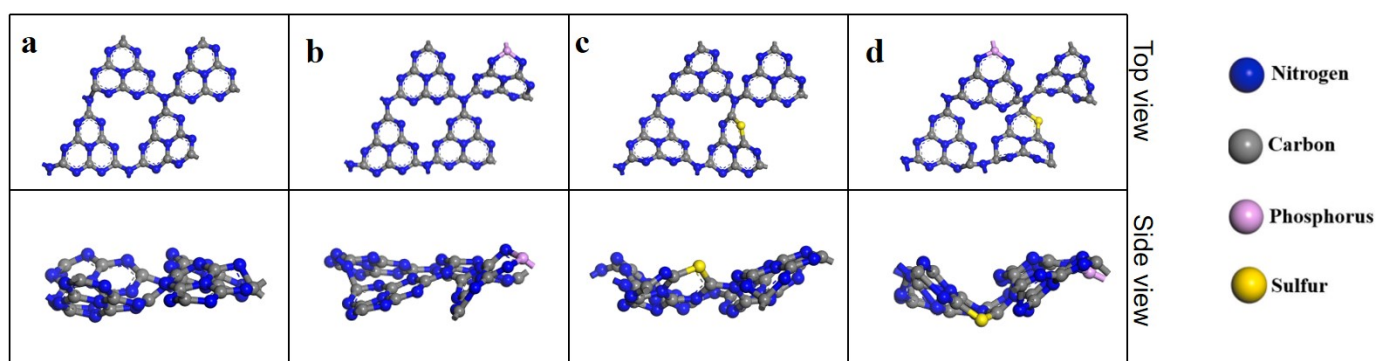
Figure S8. The top and side views of the geometric structure of the (a) pristine CN , (b) P-CN, (c) S-CN, (d) $P_{0.3}S_{0.2}$-CN.while the gray, blue, pink, and yellow balls represent the C, N, P, and S atoms.

According to the XPS results, for the P atoms, the P-N bond in the samples indicate that they were doped into the CN lattice by replacing the C atoms. While for the S atoms, the existence of S-C bonds indicates the S atoms were doped by replacing the N atoms. According to the DFT theoretical calculation from previous reports, S atoms preferentially replace N atoms at the edges of g-C₃N₄, while P atoms preferentially replace C atoms at the edges of g-C₃N₄, the C site were recognized as the optimal P doping site for its lowest formation energy, and the N site were recognized as the optimal S doping site for its lowest formation energy[4, 5].
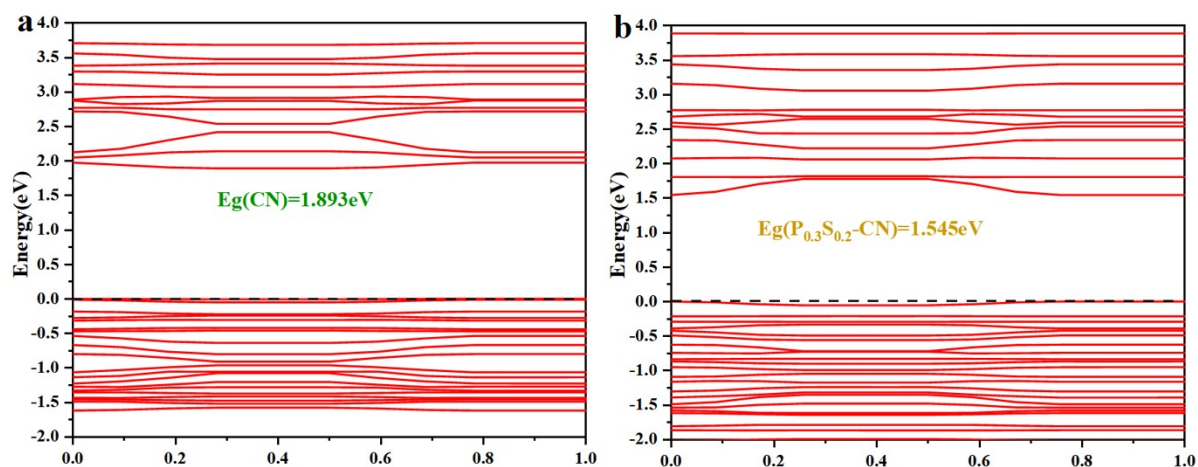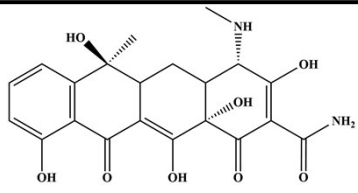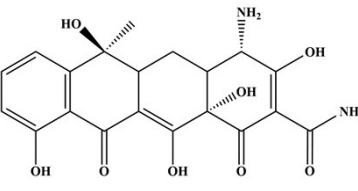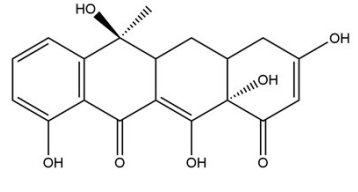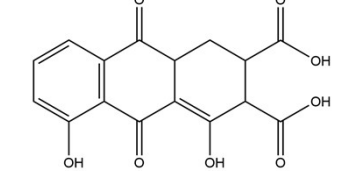
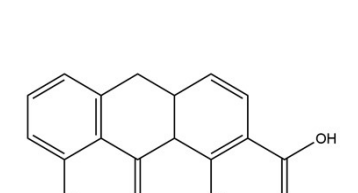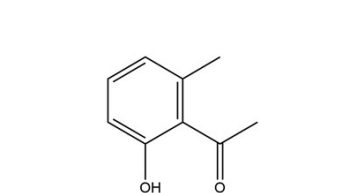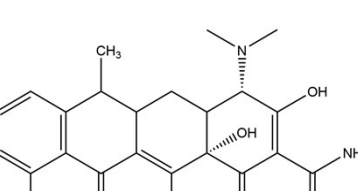Figure S9. The Band structure plots of the (a) CN and (b) $P_{0.3}S_{0.2}$-CN.

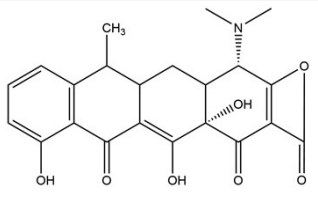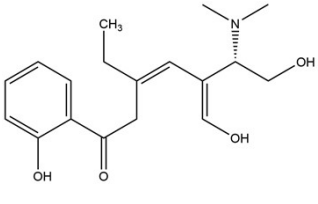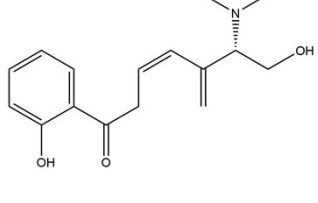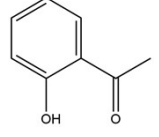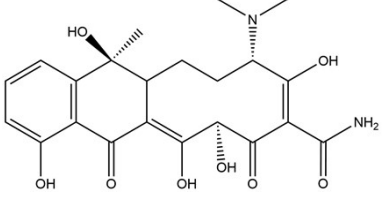Table S1. Comparison of H_2O_2 production by various photocatalysts
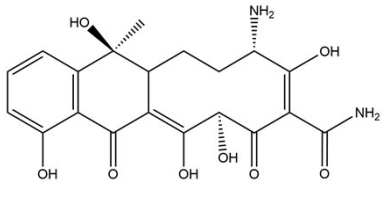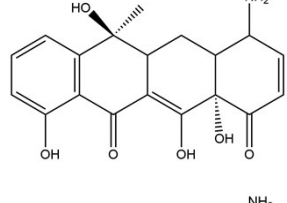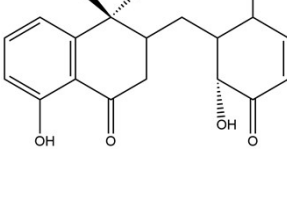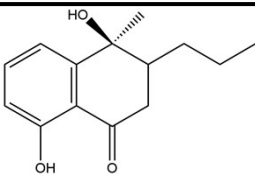
Photocatalysts	Dosage (g L^{-1})	Reaction solution	Light source	H_2O_2 production (mg L^{-1} h^{-1})	Reference
B-CNT	1	10 vol% IPA	300 W XL	31.1	[5]
Bi$_2$S$_3$@CdS@RGO	1	10 vol% IPA	300 W XL (420 nm < λ < 800 nm)	2.4	[6]
SS-CN	0.5	10 vol% IPA	300 W XL (λ > 420 nm)	2.4	[7]
KTTCN	1	0.5 vol% IPA	300 W XL (λ > 420 nm)	19.2	[8]
Ti$_3$C$_2$Mxene/porous g-C$_3$N$_4$	1	10 vol% IPA	300 W XL (λ > 420 nm)	4.47	[9]
DCN	0.83	20 vol% IPA	AM1.5 visible light (λ > 420 nm)	0.16	[10]
ZnIn$_2$S$_4$/FTCNso	0.5	10 vol% IPA	300 W XL (λ > 420 nm)	4.6	[11]
IO CN-Cv	1	10 vol% IPA	300 W XL (λ > 420 nm)	5.5	[12]

| P$_{0.3}$S$_{0.2}$-CN | 1 | 10 vol% IPA | 300 W XL (λ > 420 nm) | 28.6 | This work |

Table S2. Analysis of degradation products of TC by P$_{0.3}$S$_{0.2}$-CN photocatalyst under visible light irradiation

Products	Fragment Information (m/z)	Molecular Formula	Supposed Structure
P$_1$	430	C$_{21}$H$_{22}$N$_2$O$_8$	
P$_2$	416	C$_{20}$H$_{20}$N$_2$O$_8$	
P$_3$	358	C$_{19}$H$_{18}$O$_7$	
P$_4$	332	C$_{16}$H$_{12}$O$_8$	
P$_5$	272	C$_{15}$H$_{12}$O$_5$	
P$_6$	150	C$_9$H$_{10}$O$_2$	
P$_7$	428	C$_{22}$H$_{24}$N$_2$O$_7$	

P_8	411	$C_{22}H_{21}NO_7$	
P_9	319	$C_{18}H_{25}NO_4$	
P_{10}	275	$C_{16}H_{21}NO_3$	
P_{11}	136	$C_8H_8O_2$	
P_{12}	446	$C_{22}H_{26}N_2O_8$	
P_{13}	418	$C_{20}H_{22}N_2O_8$	
P_{14}	357	$C_{19}H_{19}NO_6$	
P_{15}	331	$C_{18}H_{21}NO_5$	
P_{16}	234	$C_{14}H_{18}O_3$	

| P$_{17}$ | 150 | C$_9$H$_{10}$O$_2$ | |
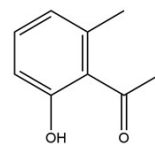
References

1 D.C. Pham, T. Cao, M.C. Nguyen, T.D. Nguyen, V.H. Nguyen, V.H. Bui and T. Nguyen, *Chem. Eng. Technol.*, 2022, **45**, 1748-1758.

2 J. Hou, D. Gao, X. Hu, L. Wang and Q. Guo, *J. Mol. Struct.*, 2023, **1275**.

3 X. Li, J. Zhang, Y. Huo, K. Dai, S. Li and S. Chen, *Appl. Catal. B-Environ.*, 2021, **280**.

4 Z. Wang, M. Chen, Y. Huang, X. Shi, Y. Zhang, T. Huang, J. Cao, W. Ho and S.C. Lee, *Appl. Catal. B-Environ.*, 2018, **239**, 352-361.

5 Y. Liu, Y. Zheng, W. Zhang, Z. Peng, H. Xie, Y. Wang, X. Guo, M. Zhang, R. Li and Y. Huang, *J. Mater. Sci. Technol.*, 2021, **95**, 127-135.

6 S.M. Ghoreishian, K.S. Ranjith, B. Park, S. Hwang, R. Hosseini, R. Behjatmanesh-Ardakani, S.M. Pourmortazavi, H.U. Lee, B. Son, S. Mirsadeghi, Y. Han and Y.S. Huh, *Chem. Eng. J.*, 2021, **419**.

7 C. Feng, L. Tang, Y. Deng, J. Wang, Y. Liu, X. Ouyang, H. Yang, J. Yu and J. Wang, *Appl. Catal. B-Environ.*, 2021, **281**.

8 J. Zhang, C. Yu, J. Lang, Y. Zhou, B. Zhou, Y.H. Hu and M. Long, *Appl. Catal. B-Environ.*, 2020, **277**.

9 Y. Yang, Z. Zeng, G. Zeng, D. Huang, R. Xiao, C. Zhang, C. Zhou, W. Xiong, W. Wang, M. Cheng, W. Xue, H. Guo, X. Tang and D. He, *Appl. Catal. B-Environ.*, 2019, **258**.

10 L. Shi, L. Yang, W. Zhou, Y. Liu, L. Yin, X. Hai, H. Song and J. Ye, *Small*, 2018, **14**.

11 Q. Liang, X. Liu, B. Shao, L. Tang, Z. Liu, W. Zhang, S. Gong, Y. Liu, Q. He, T. Wu, Y. Pan and S. Tong, *Chem. Eng. J.*, 2021, **426**.

12 J. Lei, B. Chen, W. Lv, L. Zhou, L. Wang, Y. Liu and J. Zhang, *Acs Sustain. Chem. Eng.*, 2019, **7**, 16467-16473.